



NaAlH₄ dehydrogenation properties enhanced by MnFe₂O₄ nanoparticles



Qi Wan^a, Ping Li^{a,*}, Ziliang Li^a, Kuifei Zhao^a, Zhiwei Liu^a, Ling Wang^a, Fuqiang Zhai^b,
Xuanhui Qu^{a,c}, Alex A. Volinsky^d

^a Institute for Advanced Materials and Technology, University of Science and Technology Beijing, Beijing 100083, China

^b Departament Física Aplicada, EETAC, Universitat Politècnica de Catalunya – BarcelonaTech, 08860 Castelldefels, Spain

^c State Key Laboratory for Advanced Metals and Materials, University of Science and Technology Beijing, Beijing 100083, China

^d Department of Mechanical Engineering, University of South Florida, Tampa, FL 33620, USA

HIGHLIGHTS

- Nanosized MnFe₂O₄ effect on NaAlH₄ desorption properties is studied for the first time.
- NaAlH₄ + 7 mol% MnFe₂O₄ desorption temperature onset is much lower than pristine NaAlH₄.
- The apparent activation energy of the MnFe₂O₄ doped sample is dramatically decreased.
- Mn species and Fe_{0.9536}O phases significantly improve NaAlH₄ desorption properties.

ARTICLE INFO

Article history:

Received 17 June 2013

Received in revised form

5 September 2013

Accepted 22 September 2013

Available online 2 October 2013

Keywords:

Manganese ferrite

Hydrogen storage

Sodium alanate

Dehydrogenation temperature

Apparent activation energy

ABSTRACT

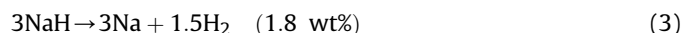
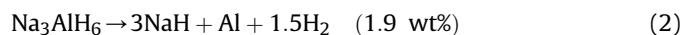
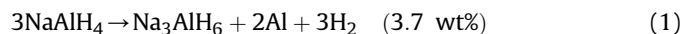
The catalytic effects of MnFe₂O₄ nanoparticles on the dehydrogenation properties of NaAlH₄, prepared by ball milling, are investigated. The onset temperatures for NaAlH₄ + 7 mol% MnFe₂O₄ are 95 °C, 152 °C and 327 °C for the three dehydrogenation steps, significantly lower compared with as-received NaAlH₄. The isothermal dehydriding kinetics shows that adding MnFe₂O₄ to NaAlH₄ could significantly enhance the desorption kinetics of NaAlH₄, 7 mol% MnFe₂O₄-doped sample also displays the well-maintained kinetics and only a slight capacity loss for the three cycles. From the differential scanning calorimetry and the Kissinger desorption kinetics analysis, the apparent activation energy of the 7 mol% MnFe₂O₄-doped sample for the three steps is 57.74 kJ mol^{−1}, 75.06 kJ mol^{−1} and 117.22 kJ mol^{−1}, resulting in 56.05 kJ mol^{−1}, 67.53 kJ mol^{−1} and 59.12 kJ mol^{−1} reduction, respectively, compared with the as-received NaAlH₄. Based on the Fourier Transform Infrared Spectroscopy, X-ray diffraction and X-ray photoelectron spectroscopy, Fe_{0.9536}O and amorphous Mn or Mn-containing species together play a synergistic role in remarkably improving NaAlH₄ dehydriding properties.

© 2013 Elsevier B.V. All rights reserved.

1. Introduction

Solid-state lightweight metal complex hydrides have received increased attention due to their high volumetric and gravimetric hydrogen storage density [1–6], which may meet the U.S. Department of Energy 2015 targets [7]. A viable hydrogen storage system requires hydrogen storage materials with more than 5.5 wt% capacity and fast desorption kinetics. Among various complex metal hydrides [1,8–17], sodium alanates are considered to be a promising solid-state hydrogen storage media, since Bogdanović and Schwickardi [18] reported that NaAlH₄ could reversibly desorb

hydrogen under moderate conditions after doping with Ti-containing catalyst. The absorption capacity decreases with the increasing of cycles, which declines from 4.2 wt% to 3.1 wt% at 170 °C under 15 MPa hydrogen pressure and from 2.7 wt% to 2.1 wt% at 200 °C under 6 MPa hydrogen pressure over 35 cycles, respectively. Upon heating, NaAlH₄ would decompose to release hydrogen in three steps according to the following reactions:



Reaction (1) happens at the temperature range of 170–230 °C, reactions (2) and (3) initiate above 250 °C and 400 °C, respectively.

* Corresponding author.

E-mail address: ustbliping@126.com (P. Li).

However, high desorption temperature, sluggish dehydrogenation kinetics and poor reversibility limit NaAlH₄ practical applications [6,19–21]. During the past decade researchers have been trying to overcome these drawbacks. The efforts included preparing nanocrystalline NaAlH₄ [6,22–24], and adding metal catalysts [25–29], C species [20,30,31], metal halides [21,32–37], metal oxides [2,5,19,38–40] and other compounds [3,41–43]. For improvement of dehydrogenating properties of NaAlH₄, generally, metal halides have better catalytic effect than metal oxides, metal oxides have better catalytic effect than metals, but some metal oxide has better catalytic effect than metal halide, such as Nb₂O₅ > NbF₅. Usually, the dehydrogenating temperature and dehydrogenating kinetics can be strikingly improved by adding catalyst, but the dehydrogenating capacity decreases remarkably with the increase of cycles [2,27,47]. Naik et al. demonstrated the superior effects of Mn²⁺ on improving the dehydrogenation properties of NaAlH₄ [35]. It was also reported that Fe and Fe³⁺ could ameliorate NaAlH₄ hydrogen storage performance [29,44]. Moreover, Zhai et al. [45] reported that MnFe₂O₄ could remarkably improve LiAlH₄ dehydrogenation. MnFe₂O₄ has better catalytic effect than Fe or Mn oxides alone in improving the dehydrogenating properties of LiAlH₄. NaAlH₄ has similar performances with LiAlH₄. Therefore, it is reasonable to assume that MnFe₂O₄ would show great potential as a catalyst to advance NaAlH₄ hydrogen storage performance. Motivated by the above findings, in the present work, MnFe₂O₄ nanoparticles were employed as catalyst precursors to study their effect on the dehydrogenation properties of NaAlH₄ prepared by ball milling.

2. Experimental

NaAlH₄ (≥93% purity) was purchased from Sigma Aldrich Co., and MnFe₂O₄ (≥99.99% purity, 20 nm particle size) was prepared by the nitrate–citrate auto-combustion methods. The details of the preparation procedure are given in the previous report [46]. Both materials were used directly, without any further purification. All handling (including weighing and loading) was performed in a high-purity argon-filled glove box in order to avoid oxidation and moisture. About 3 g of NaAlH₄ was mixed with different mole fractions (3 mol%, 5 mol%, 7 mol%, and 9 mol%) of MnFe₂O₄ nanoparticles, and then ball milled for 30 min in a high-energy Spex Mill. All the samples were loaded into the stainless steel vial in an argon-filled glove box. ZrO₂ balls were added with a ball-to-powder weight ratio of 15:1. The samples were ball milled for 10 min and then cooled down for 5 min after each cycle.

The dehydrogenation properties of as-received NaAlH₄ and doped samples were measured using a pressure–composition–temperature (PCT) apparatus (Beijing Nonferrous Metal Research Institute, China). For non-isothermal dehydrogenation, 0.5 g of the sample was loaded into the vessel, and then heated up to 500 °C at a 4 °C min^{−1} rate under 0.01 MPa atm pressure. The isothermal dehydrogenation measurements for the undoped and doped samples were performed at 120 °C and 150 °C under a hard vacuum atmosphere. Following the first complete dehydrogenation, the samples were subjected to rehydrogenation studies at 150 °C under 5 MPa hydrogen pressure for 180 min. Subsequently, the rehydrogenated samples were dehydrogenated at similar temperature.

In order to further analyze the dehydrogenation performance and calculate the desorption activation energy of the doped NaAlH₄ sample by means of the Kissinger method, the differential scanning calorimetry (DSC) was performed using NETZSCH STA 449C in high-purity argon (50 mL min^{−1} flow rate, 99.999% pure). About 5 mg of the sample was sealed into a 50 mL alumina crucible in the glove box, and then heated at different rates (4 °C min^{−1}, 7 °C min^{−1} and 10 °C min^{−1}), from 50 °C to 500 °C.

The morphology of the as-received and doped samples after ball milling was examined by scanning electron microscopy (SEM, ZEISS EVO18, Germany). The phase structure of the samples after ball milling and after dehydrogenation was determined by using the MXP21VAHF X-ray diffractometer (XRD with Cu K α radiation, 40 kV, 200 mA) at room temperature. The 2 θ angle was varied from 25° to 90° in 0.02° increments, 1 s per step. The samples were covered with the paraffin film to prevent oxidation during the XRD test.

Fourier transformation infrared spectroscopy was performed by using an infrared spectrophotometer (NEXUS670). The spectral resolution was 4 cm^{−1}. Scans were performed between 500 cm^{−1} and 2000 cm^{−1} in argon. X-ray photoelectron spectroscopy (XPS) experiments were performed in an ultra high vacuum (UHV) chamber with the base pressure of around 3 × 10^{−13} Pa, equipped with a Perkin–Elmer PHI-5300 XPS spectrometer.

3. Results and discussion

3.1. Dehydrogenation temperature

Fig. 1 shows the non-isothermal desorption curves of as-received NaAlH₄, as-milled NaAlH₄ and ball-milled NaAlH₄ doped with 3 mol%, 5 mol%, 7 mol% and 9 mol% MnFe₂O₄ nanopowders. The desorption curves clearly reveal that adding MnFe₂O₄ nanoparticles dramatically improves NaAlH₄ dehydrogenating properties, resulting in a striking reduction of the onset desorption temperature, not only for the first and second steps, but also for the third step. The onset desorption temperature for all doped samples is below 130 °C, indicating a significant decrease compared with the as-received NaAlH₄. For the as-received NaAlH₄, it starts to decompose at 179 °C, and weight loss is about 5.18 wt% after heating to 290 °C. The third step commences at 411 °C, and a hydrogen release capacity of 6.4 wt% is obtained below 450 °C. Compared with as-received NaAlH₄, the onset desorption temperature of as-milled NaAlH₄ decreased slightly by 14 °C, 11 °C and 13 °C for the three steps, respectively, due to the NaAlH₄ activation introduced by the ball milling [2,36].

When doping MnFe₂O₄ nanoparticles to the NaAlH₄ matrix, the onset desorption temperature of NaAlH₄ is further reduced. For the 3 mol% doped sample, the dehydrogenation process starts at 125 °C for the first stage, and initiates at 180 °C and 367 °C for the second

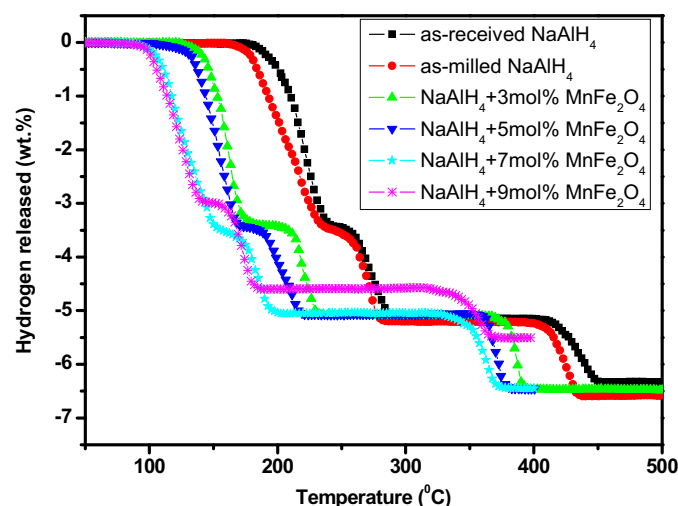


Fig. 1. Thermal desorption curves of the as-received NaAlH₄, as-milled NaAlH₄ and ball-milled NaAlH₄ doped with 3 mol%, 5 mol%, 7 mol% and 9 mol% nanosized MnFe₂O₄.

and the third steps, respectively. Further increase of the additives amount to 5 mol% reduces the onset dehydrogenation temperature to 115 °C for the first stage. Compared with as-received NaAlH₄, adding 3 mol% and 5 mol% of MnFe₂O₄ causes a reduction in the onset desorption temperature of 54 °C and 64 °C for the first step, 60 °C and 75 °C for the second step, and 44 °C and 56 °C for the third step, respectively. During the three dehydrogenation processes, the sample with 3 mol% MnFe₂O₄ releases about 3.42 wt% hydrogen for the first stage, 5.12 wt% hydrogen for the first two stages, 6.79 wt% hydrogen for three stages, whereas 3.41 wt%, 5.10 wt%, and 6.75 wt% hydrogen is desorbed for these of the 5 mol% doped sample, respectively. 7 mol% MnFe₂O₄ has the onset temperatures for the three steps of 95 °C, 152 °C and 327 °C, respectively, resulting in further decrease, compared with the 3 mol% and 5 mol% doped samples, and a reduction of 84 °C, 88 °C and 84 °C, respectively, compared with the as-received NaAlH₄. Meanwhile, the 7 mol% doped sample releases 3.40 wt%, 5.08 wt%, and 6.71 wt% hydrogen in the first step, the first two steps, and three dehydrogenation steps, respectively. With the MnFe₂O₄ amount increasing to 9 mol%, the onset dehydrogenation temperature reduces to 90 °C, 140 °C and 319 °C, respectively, which demonstrates MnFe₂O₄ superiority in improving the NaAlH₄ desorption temperature, compared with other various catalysts reported in the literature [2,5,31,33,35,36,40,47]. However, the desorption hydrogen content for the 9 mol% doped sample is only 2.89 wt%, 4.59 wt%, and 5.51 wt% for the first step, the first two steps, and the three steps, respectively, signifying a drastic reduction in the released hydrogen capacity due to an excess amount of MnFe₂O₄ nanoparticles. The decrease in hydrogen storage capacity may be associated with the impurity in the original NaAlH₄ powder, the amount of catalyst, and some partial decomposition of NaAlH₄ during high-energy ball milling with MnFe₂O₄ nanoparticles, despite the air-cooling of the vial employs during the milling process, the localized impact associated with the ball milling induces the localized temperature increase of the NaAlH₄ powders being ball-milled and heavily catalyzed with MnFe₂O₄ nanoparticles. We assume that the simultaneous effect of both the temperature increase during milling and catalyst causes the partial decomposition of NaAlH₄. For the small additions, the loss in capacity is insignificant owing to the moderate exposure of NaAlH₄ to catalyst, as reported in the literature [36,45,48]. Therefore, the NaAlH₄ + 7 mol% MnFe₂O₄ sample exhibits optimal dehydrogenation performance, including the onset dehydrogenation temperature and the released hydrogen capacity. Thus, using the optimal 7 mol% amount of MnFe₂O₄ nanoparticles, allows analyzing the MnFe₂O₄ mechanism and the catalytic effect in the following tests.

To further compare the thermal decomposition behavior of NaAlH₄, with and without MnFe₂O₄ doping, Fig. 2 shows DSC curves of the as-received NaAlH₄ and NaAlH₄ doped with 7 mol% MnFe₂O₄ samples within the 50–500 °C temperature range (4 °C min⁻¹ heating rate). As presented in Fig. 2(a), the DSC curve of the as-received NaAlH₄ includes six distinct peaks, corresponding to one exothermic process and five endothermic processes. The first exothermic process appears at 173.1 °C, corresponding to the interaction of NaAlH₄ with surface hydroxyl impurities, as reported in other papers [2,48,49]. The first endothermic peak at 182.5 °C arises from NaAlH₄ melting [36,43]. The second endothermic peak occurs at 239.6 °C due to dehydrogenation of NaAlH₄ to Na₃AlH₆. The third endothermic peak at 252.6 °C can be attributed to a phase transition of α -Na₃AlH₆ to β -Na₃AlH₆ [2,36]. The fourth and fifth endothermic peaks at 270.4 °C and 433.5 °C are assigned to the dehydrogenation of Na₃AlH₆ and NaH, respectively. In contrast, the features of the MnFe₂O₄-doped sample composite are strikingly different, displaying only three characteristic endothermic peaks in the DSC plot seen in Fig. 2(b). These three endothermic peaks at

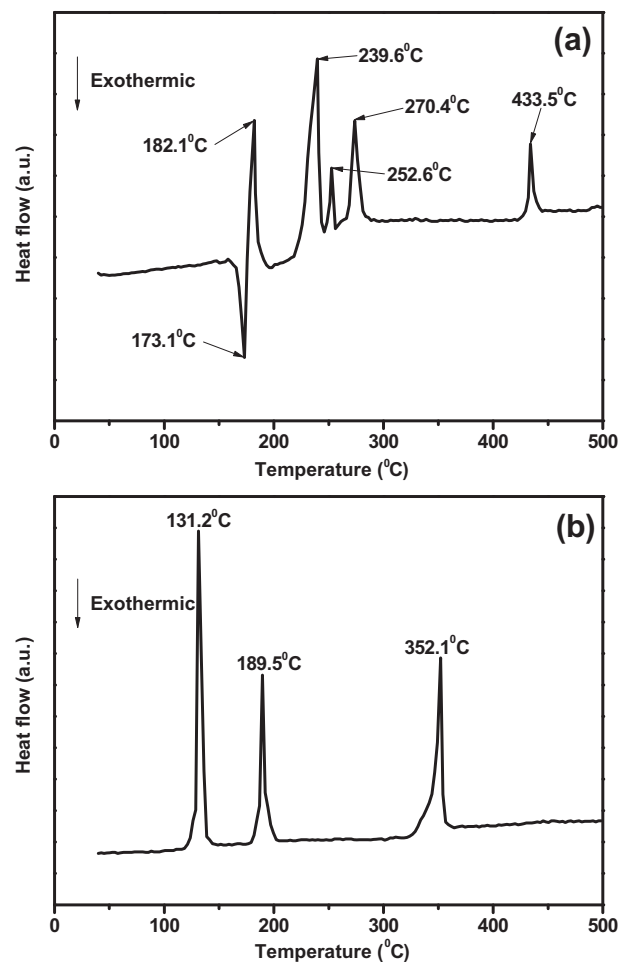


Fig. 2. DSC profiles of (a) as-received NaAlH₄ and (b) ball-milled NaAlH₄ doped with 7 mol% MnFe₂O₄ within the 50–500 °C temperature range (4 °C min⁻¹ heating rate).

131.2 °C, 189.5 °C and 352.1 °C correspond to the dehydrogenation of NaAlH₄, Na₃AlH₆ and NaH, respectively, which is similar with the DSC results of NaAlH₄ doped with various catalysts reported in the literature [3,35,36,47,50–55].

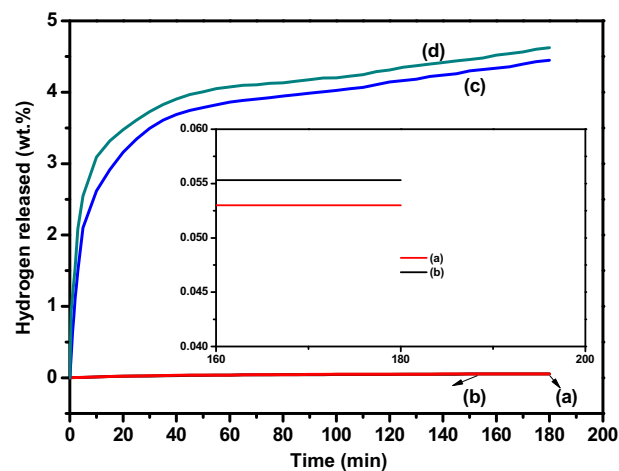


Fig. 3. Isothermal desorption curves of (a) as-received NaAlH₄ at 150 °C, (b) as-milled NaAlH₄ at 150 °C, and ball-milled NaAlH₄ doped with 7 mol% MnFe₂O₄ at (c) 120 °C and at (d) 150 °C.

The notable reduction of the peak temperature in the above DSC results shows that the dehydrogenation properties of NaAlH₄ are significantly improved by adding nanosized MnFe₂O₄. Nevertheless, it is noteworthy that the desorption temperature onset measured by DSC is quite higher than that measured by PCT. A similar phenomenon is also reported in the literature [2,3,36]. This is mainly due to the different dehydrogenation atmospheres for the samples tested with DSC (0.1 MPa argon) and PCT (0.01 MPa atm), resulting in different driving forces during the dehydriding process.

3.2. Dehydrogenation kinetics

The excellent effect of MnFe₂O₄ nanopowders on promoting the dehydriding kinetics of NaAlH₄, in comparison with the as-received NaAlH₄ and as-milled NaAlH₄ samples, is further demonstrated by examination of isothermal hydrogen desorption at different temperatures (Fig. 3). Fig. 3 shows isothermal desorption kinetics curves of as-received NaAlH₄ and as-milled NaAlH₄ at 150 °C and NaAlH₄ + 7 mol% MnFe₂O₄ samples at 120 °C and 150 °C, respectively. For the as-received NaAlH₄ and as-milled NaAlH₄, only 0.05 wt% hydrogen is released at 150 °C after 180 min for both samples, indicating poor dehydriding kinetics of as-received NaAlH₄ and as-milled NaAlH₄. However, NaAlH₄ + 7 mol% MnFe₂O₄ releases 4.43 wt% hydrogen at 120 °C in 180 min. Further temperature increase to 150 °C results in 4.67 wt% of released hydrogen for the same time. Moreover, the doped sample desorbs about 3.11 wt% hydrogen in 10 min at 150 °C, which demonstrates MnFe₂O₄ superiority in improving NaAlH₄ desorption kinetics, compared with other catalysts reported in the literature [2,3,5,26,36]. Therefore, dramatic improvement of NaAlH₄ dehydrogenation kinetics can be achieved by adding MnFe₂O₄ nanopowders.

Further study indicates that the catalytic enhancement arising upon adding MnFe₂O₄ persists well in dehydrogenation/rehydrogenation cycles. Fig. 4 brings out the results of the first three rehydrogenations of 7 mol% MnFe₂O₄-doped sample at 150 °C under 5 MPa hydrogen pressure for 180 min. 7 mol% MnFe₂O₄-doped sample exhibits a slow decrease in hydrogen absorption capacity, from about 3.90 wt% to about 3.81 wt% in the three cycles. The dehydriding curves of ball-milled NaAlH₄ doped with 7 mol% MnFe₂O₄ at 150 °C after the rehydrogenation are shown in Fig. 5. 7 mol% MnFe₂O₄-doped sample also displays the well-maintained kinetics and only a slight capacity loss for the three cycles, it declines from 3.76 wt% to 3.64 wt% in 180 min. Thus, dramatic

improvement of NaAlH₄ rehydrogenation/dehydrogenation properties can be achieved by adding MnFe₂O₄ nanopowders.

3.3. Dehydrogenation mechanism

SEM images of the as-received NaAlH₄ and the ball-milled NaAlH₄ sample doped with 7 mol% MnFe₂O₄ nanopowders are presented in Fig. 6. The particle size of the as-received NaAlH₄ is larger than 100 μm, however, the particle size of the MnFe₂O₄-doped sample is between 3 μm and 8 μm. It must be mentioned that the embedded MnFe₂O₄ particles cannot be seen on the NaAlH₄ surface by SEM because of their extremely small size. The dehydriding properties of NaAlH₄ doped with MnFe₂O₄ are significantly improved after ball milling due to the decreased particle size, which results in high surface defect density and more grain boundaries. Moreover, a high density of nanosized catalyst particles forms a large number of nucleation sites at the surface of the NaAlH₄ matrix, leading to surface activation and larger surface area of the NaAlH₄ particles.

In order to further analyze NaAlH₄ desorption mechanism after doping with MnFe₂O₄, the apparent activation energies, E_a , corresponding to NaAlH₄, NaAlH₆ and NaH decomposition, for both undoped and doped NaAlH₄ samples, are obtained from DSC data by using the Kissinger method. Fig. 7 shows the Kissinger plots of as-received NaAlH₄ and 7 mol% MnFe₂O₄-doped sample. The E_a values of as-received NaAlH₄ for the three steps are 113.79 kJ mol⁻¹, 142.59 kJ mol⁻¹ and 176.34 kJ mol⁻¹, respectively, while the E_a of the MnFe₂O₄-doped sample for the three dehydrogenation steps are calculated to be 57.74 kJ mol⁻¹, 75.06 kJ mol⁻¹ and 117.22 kJ mol⁻¹, respectively. Therefore, there is a remarkable reduction of 56.05 kJ mol⁻¹, 67.53 kJ mol⁻¹ and 59.12 kJ mol⁻¹ in E_a for the three dehydrogenation steps of NaAlH₄, indicating that the apparent activation energy is significantly improved by adding MnFe₂O₄ nanoparticles. To demonstrate MnFe₂O₄ catalytic effect on NaAlH₄ dehydrogenation, comparison of E_a for NaAlH₄ doped with different catalysts is summarized in Table 1 [2,3,26,33,36,40,43]. MnFe₂O₄-doped samples have the lowest apparent activation energy values for the three dehydriding processes, which signifies MnFe₂O₄ superiority in improving the desorption performance of NaAlH₄, compared with other reported catalysts.

The FTIR spectra of the as-milled NaAlH₄, and 3 mol% and 7 mol% MnFe₂O₄ doped NaAlH₄ samples after ball milling are compared in Fig. 8. It is clear that there is an IR absorption peak at 1440 cm⁻¹

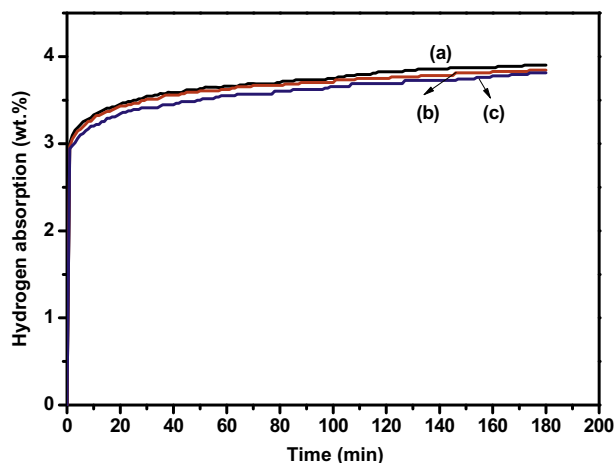


Fig. 4. Rehydrogenation curves of ball-milled NaAlH₄ doped with 7 mol% MnFe₂O₄ at 150 °C under 5 MPa hydrogen pressure during the first three cycles, (a) the first rehydrogenation, (b) the second rehydrogenation and (c) the third rehydrogenation.

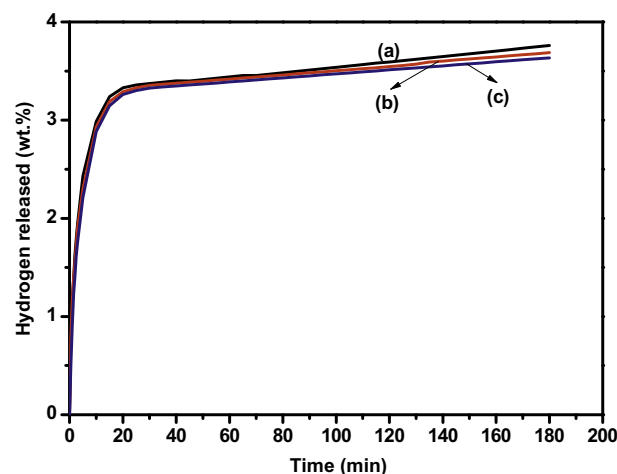


Fig. 5. Dehydriding curves of ball-milled NaAlH₄ doped with 7 mol% MnFe₂O₄ at 150 °C after the rehydrogenation, (a) after the first rehydrogenation, (b) after the second rehydrogenation, and (c) after the third rehydrogenation.

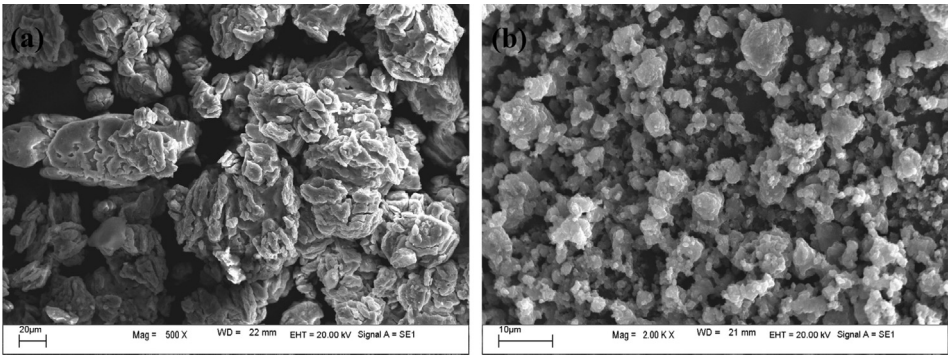


Fig. 6. SEM images of (a) as-received NaAlH₄ and (b) ball-milled NaAlH₄ doped with 7 mol% MnFe₂O₄.

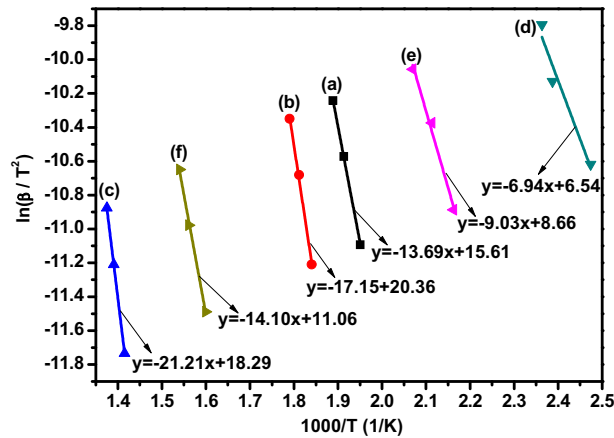


Fig. 7. Kissinger plots for the as-received NaAlH₄ (a) the first step, (b) the second step, and (c) the third step and ball-milled NaAlH₄ doped with 7 mol% MnFe₂O₄, (d) the first step, (e) the second step, and (f) the third step.

for the doped samples. Moreover, the intensity of the IR absorption peak at 1440 cm⁻¹ gradually becomes stronger with the increase of MnFe₂O₄ amount, which could be ascribed to the appearance of Al–H stretching mode of Na₃AlH₆ [2,41,56]. However, no IR absorption peak exists at the same position in the FTIR spectra of the as-milled NaAlH₄ in Fig. 8. For the as-milled NaAlH₄, there are two regions of active infrared vibrations of the Al–H bonds: Al–H stretching mode between 1600 and 1700 cm⁻¹ and H–Al–H bending modes between 600 and 900 cm⁻¹ [26,35,36,41,57].

Na₃AlH₆ also exhibits two regions of active infrared vibrations: Al–H stretching modes between 1200 and 1500 cm⁻¹ and H–Al–H bending modes between 600 and 1000 cm⁻¹ [2,41,56]. Therefore, it is reasonable to conclude that the doped NaAlH₄ sample incurs partial decomposition and yields Na₃AlH₆ during the ball milling process, and the decomposition reaction is processed more severely with the increasing MnFe₂O₄ content.

To illustrate that NaAlH₄ and MnFe₂O₄ react during ball milling, Fig. 9 shows XRD patterns of the as-received NaAlH₄ (Fig. 9(a)), as-

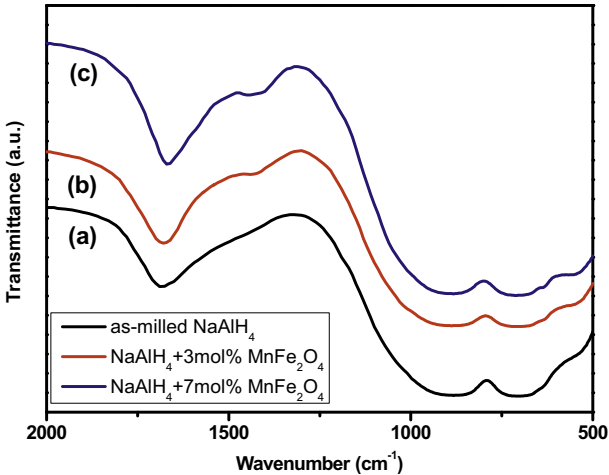


Fig. 8. FTIR spectra of (a) as-milled NaAlH₄ and ball-milled NaAlH₄ doped with (b) 3 mol% and (c) 7 mol% MnFe₂O₄.

Table 1
Activation energy of NaAlH₄ doped with different catalysts.

| Catalyst | First stage E_a (kJ mol ⁻¹) | | Second stage E_a (kJ mol ⁻¹) | | Third stage E_a (kJ mol ⁻¹) | | Reference |
|----------------------------------|---|--------------|--|--------------|---|---------------|-----------|
| | Before doping | After doping | Before doping | After doping | Before doping | After doping | |
| TiO ₂ | 116 | 73 | 149 | 101 | 180 | 142 | [2] |
| Nb ₂ O ₅ | 116 | 65 | 149 | 85 | 180 | 131 | [2] |
| TiB ₂ | 118.1 | 106.5 | 120.7 | 105.5 | — | — | [3] |
| CeCl ₃ | 114.2 | 80.76 | 156.8 | 97.27 | — | — | [33] |
| CeAl ₄ | 114.2 | 80.93 | 156.8 | 98.94 | — | — | [33] |
| Co–B | — | 67.95 | — | — | — | — | [26] |
| LaCl ₃ | 114.2 | 86.38 | 162.6 | 96.11 | — | — | [43] |
| La ₃ Al ₁₁ | 114.2 | 92.95 | 162.6 | 99.27 | — | — | [43] |
| SmCl ₃ | 114.2 | 88.96 | 162.6 | 96.77 | — | — | [43] |
| SmAl ₃ | 114.2 | 91.87 | 162.6 | 98.94 | — | — | [43] |
| NbF ₅ | 118.2 | 88.2 | 120.9 | 102.9 | — | — | [36] |
| Ti | 119 | 77 | — | — | — | — | [40] |
| TiO ₂ | 119 | 67 | — | — | — | — | [40] |
| MnFe ₂ O ₄ | 113.79 ± 0.09 | 57.74 ± 1.47 | 142.59 ± 0.88 | 75.06 ± 0.87 | 176.34 ± 0.08 | 117.22 ± 0.68 | This work |

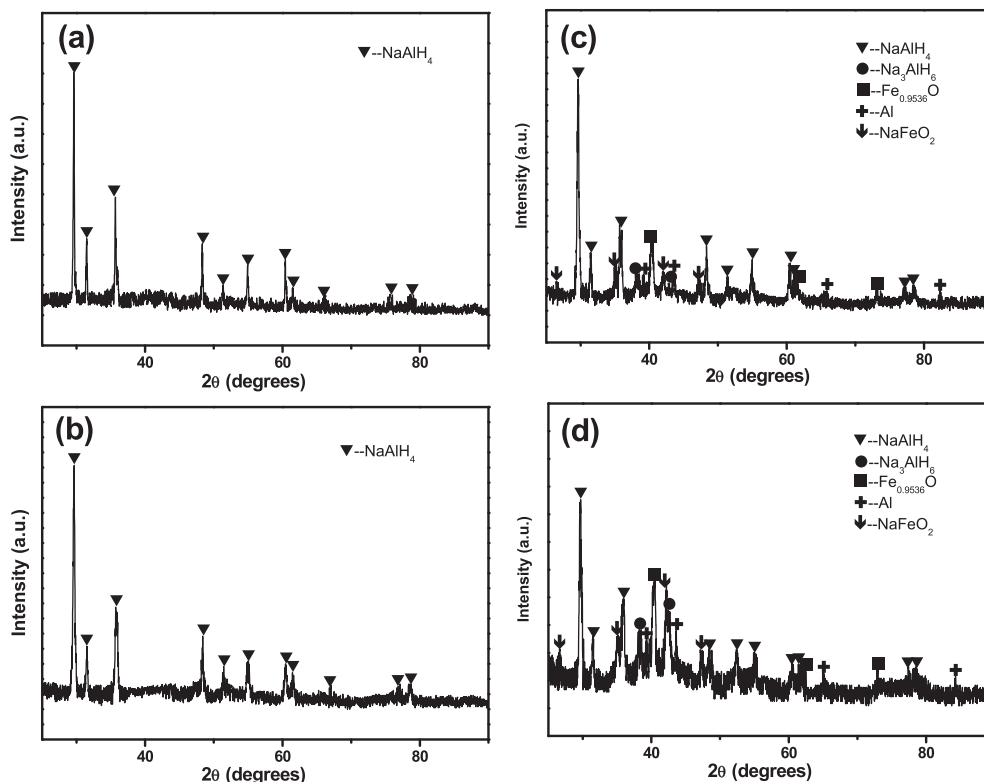
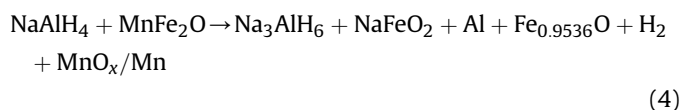


Fig. 9. XRD patterns of (a) as-received NaAlH₄, (b) as-milled NaAlH₄, and ball-milled NaAlH₄ doped with (c) 3 mol% and (d) 7 mol% MnFe₂O₄.

milled NaAlH₄ (Fig. 9(b)) and NaAlH₄ doped with 3 mol% (Fig. 9(c)) and 7 mol% (Fig. 9(d)) MnFe₂O₄ after ball milling. For the as-received and as-milled NaAlH₄, all diffraction peaks correspond to NaAlH₄, and no additional diffraction peaks are detected, indicating that NaAlH₄ remains stable during the ball milling process. The stability of NaAlH₄ could also be confirmed by the FTIR spectra of as-milled NaAlH₄ (Fig. 8). Compared with as-received NaAlH₄, diffraction peaks of as-milled NaAlH₄ and the doped samples are considerably broadened as a consequence of particle size reduction (also confirmed by SEM), more defects and mechanical strain created within the lattice by ball milling. For the doped samples after ball milling, new phases of Al and Na₃AlH₆ start to appear after adding 3 mol% MnFe₂O₄. At the same time, the diffraction peaks of NaFeO₂ and Fe_{0.9536}O are observed, for the doped samples in Fig. 9, which indicates that the reaction between NaAlH₄ and MnFe₂O₄ takes place during ball milling. A similar decomposition reaction occurs between NaAlH₄ and Nb₂O₅ [2]. With further increase of the MnFe₂O₄ amount, peak intensities of the decomposition products, including Al, Na₃AlH₆, NaFeO₂ and Fe_{0.9536}O gradually increase, but NaAlH₄ peak intensities decline, suggesting that NaAlH₄ reacts with MnFe₂O₄ and experiences partial decomposition during ball milling, which becomes more severe with increasing MnFe₂O₄ amount. The diffraction peaks of MnFe₂O₄ are not detected for all doped samples. It is difficult for the MnFe₂O₄ nanoparticles to be distinguished from the noisy background signal, mainly because of their extremely small particle sizes, high dispersion and relatively lower content, resulting in their intrinsically weak X-ray signal, compared with NaAlH₄ powders. This phenomenon is in accordance with the reported literature results that TiO₂- [2,39,40] and NbF₅-doped [36] NaAlH₄, as also no additives can be detected for those samples after ball milling. It is noteworthy that, although NaAlH₄ reacts with MnFe₂O₄ and forms NaFeO₂ and Fe_{0.9536}O as the decomposition products, there are no diffraction peaks of Mn or Mn-containing

species in Fig. 9. It is believed to be mainly due to Mn or Mn-containing phases being in an amorphous state [20,36,49]. It can be concluded that the reaction between NaAlH₄ and MnFe₂O₄ during ball milling may be as follows:



In order to determine the phase structures of the doped NaAlH₄ samples in the dehydrogenation process, XRD scans are performed on the as-milled NaAlH₄ (Fig. 10(a)) as well as 3 mol% (Fig. 10(b)) and 7 mol% (Fig. 10(c)) MnFe₂O₄-doped samples after complete desorption, as shown in Fig. 10. For the as-milled NaAlH₄, the XRD pattern shows that the sample only has Na and Al phases after desorption. For the doped samples, the XRD patterns imply that there are not only Na and Al phases, but also NaFeO₂ and Fe_{0.9536}O phases. The Fe_{0.9536}O reflections intensity gradually increases with the amount of MnFe₂O₄. Considering the extreme improvement of NaAlH₄ desorption properties by doping MnFe₂O₄ nanoparticles, in-situ formed Fe_{0.9536}O acts as a catalyst for NaAlH₄ desorption. Meanwhile, although no diffraction peaks of Mn or Mn-containing species could be detected for the doped samples in Fig. 10, it is reasonable to conclude that the Mn or Mn-containing species may also play an important catalytic role for NaAlH₄ during the dehydrogenation process.

XPS spectroscopy of MnFe₂O₄-doped NaAlH₄ is carried out to investigate the nature of the Mn and Fe species after milling. Fig. 11 shows the XPS narrow scan spectra of the ball-milled NaAlH₄ doped with 7 mol% MnFe₂O₄. Fig. 11(a) shows the photoemission spectrum of Fe 2p at 707.0 eV and 711.8 eV, corresponding to Fe_xO_y and NaFeO₂, respectively. Fig. 11(b) shows the photoemission spectrum

of Mn 2p, which is composed of Mn 2p_{3/2} and Mn 2p_{1/2} with the binding energy of 640 eV and 652.9 eV, respectively, corresponding to MnO_x/Mn. XPS results further confirm that NaAlH₄ and MnFe₂O₄ react during ball milling.

Based on the analysis above, it can be concluded that MnFe₂O₄ is not the real catalyst, intermediate phases NaFeO₂, Fe_{0.9536}O and amorphous MnO_x/Mn formed during ball milling together play a

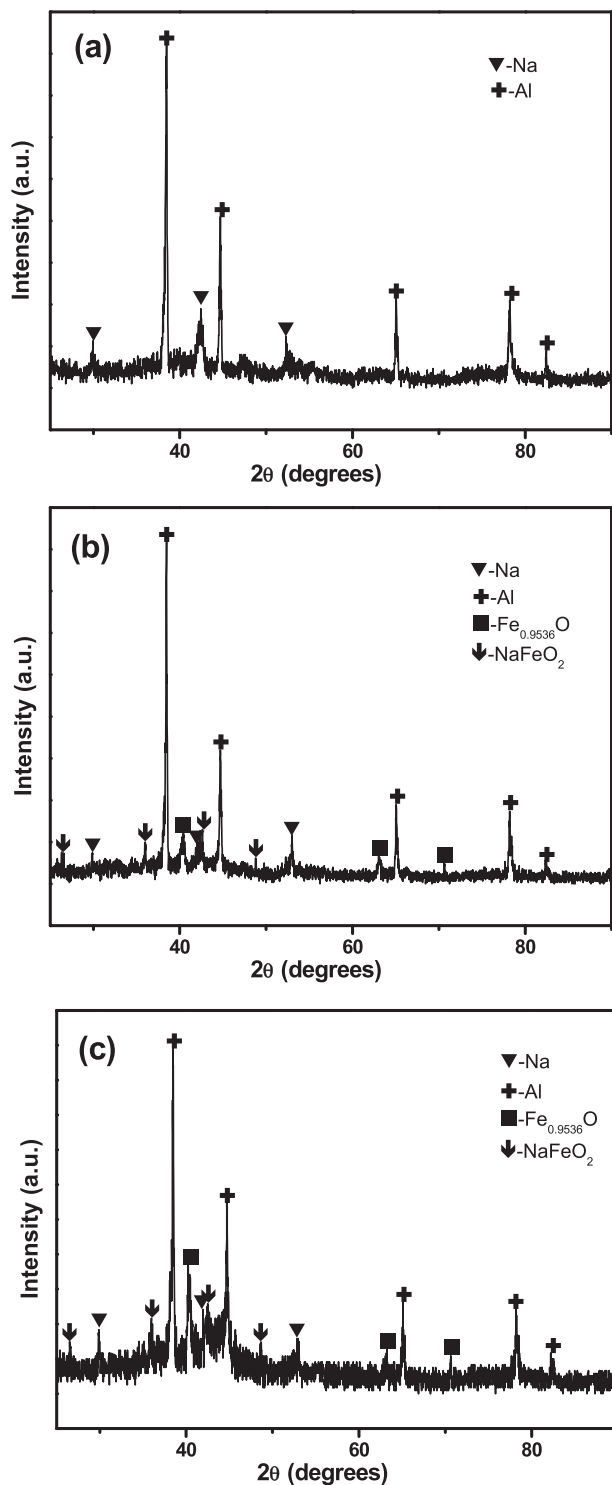


Fig. 10. XRD patterns of (a) as-milled NaAlH₄, ball-milled NaAlH₄ doped with (b) 3 mol % and (c) 7 mol% MnFe₂O₄ after desorption.

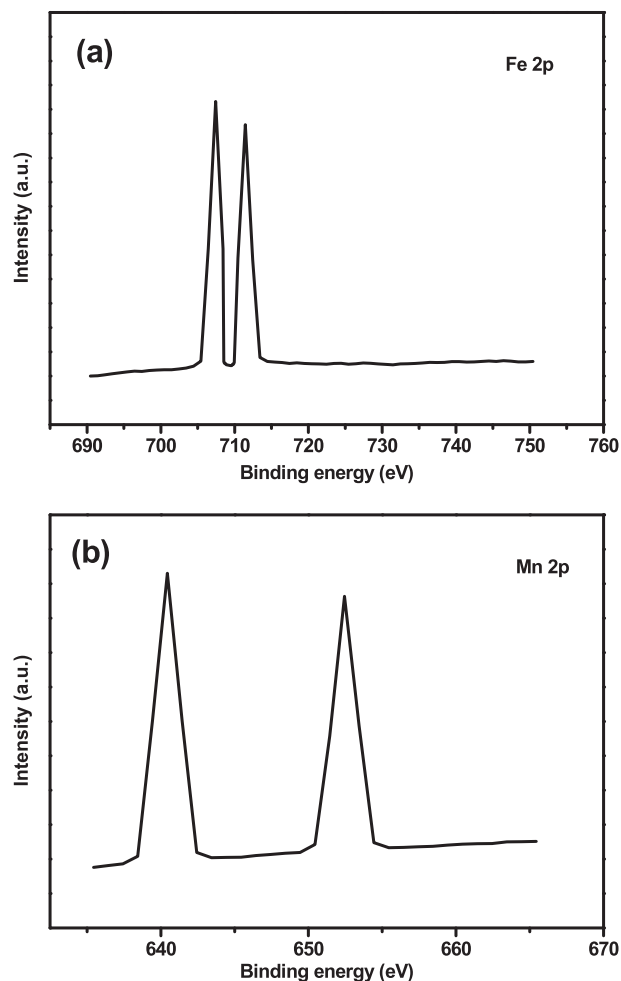


Fig. 11. Narrow scan XPS spectra of NaAlH₄ doped with 7 mol% MnFe₂O₄ after ball milling (a) Fe 2p and (b) Mn 2p.

synergistic role in remarkably improving dehydrogenation properties of NaAlH₄.

4. Conclusions

In conclusion, the dehydrogenation properties of NaAlH₄ are remarkably improved by adding MnFe₂O₄ nanoparticles. The onset desorption temperature of the ball-milled NaAlH₄ doped with 7 mol% MnFe₂O₄ is 95 °C, 152 °C and 327 °C for the three steps, releasing 6.71 wt% hydrogen, resulting in 84 °C, 88 °C and 84 °C decrease, respectively, compared with the as-received NaAlH₄. The isothermal dehydriding kinetics shows that 7 mol% MnFe₂O₄-doped sample can release 4.43 wt% at 120 °C in 180 min. When temperature is increased up to 150 °C, 4.67 wt% is released in 180 min, whereas as-received NaAlH₄ only releases 0.05 wt% hydrogen for the same conditions (time and temperature). 7 mol% MnFe₂O₄-doped sample also displays the well-maintained kinetics and only a slight capacity loss for the three cycles. This demonstrates that adding MnFe₂O₄ to NaAlH₄ significantly reduces the decomposition temperature and enhances the desorption kinetics of NaAlH₄. From the differential scanning calorimetry and the Kissinger desorption kinetics analysis, the apparent activation energy values of the 7 mol% MnFe₂O₄-doped sample for the three steps are 57.74 kJ mol⁻¹, 75.06 kJ mol⁻¹ and 117.22 kJ mol⁻¹, resulting in 56.05 kJ mol⁻¹, 67.53 kJ mol⁻¹ and 59.12 kJ mol⁻¹ reduction, respectively, compared with the as-received NaAlH₄.

sample. Based on Fourier Transform Infrared Spectroscopy, X-ray diffraction and X-ray photoelectron spectroscopy, NaFeO_2 , $\text{Fe}_{0.9536}\text{O}$ and amorphous Mn or Mn-containing species together play a synergistic role in remarkably improving dehydrogenation properties of NaAlH_4 .

Acknowledgments

The authors acknowledge the financial support from the National High-Tech R&D Program (863 Program) of China (2006AA05Z132).

References

- [1] I.P. Jain, P. Jain, A. Jain, *J. Alloys Compd.* 503 (2010) 303–339.
- [2] Rafi-ud-din, X.H. Qu, P. Li, Z. Lin, Q. Wan, M.Z. Iqbal, M.Y. Rafique, *J. Phys. Chem. C* 116 (2012) 11924–11938.
- [3] L. Li, F.Y. Qiu, Y.J. Wang, G. Liu, C. Yan, C.H. An, Y.A. Xu, Y.P. Wang, D.W. Song, L.F. Jiao, H.T. Yuan, *Mater. Chem. Phys.* 134 (2012) 1197–1202.
- [4] S.L. Liu, Q.H. Ma, Z.Z. Liu, X.P. Zheng, *Rare Met. Mater. Eng.* 40 (2011) 2083–2087.
- [5] J. Ma, J. Li, R.Y. Tang, D.W. Li, W.Z. Li, Q.Y. Chen, *Int. J. Hydrogen Energy* 36 (2011) 9091–9097.
- [6] X.L. Fan, X.Z. Xiao, J. Shao, L.T. Zhang, S.Q. Li, H.W. Ge, Q.D. Wang, L.X. Chen, *Nano Energy* (2013), <http://dx.doi.org/10.1016/j.nanoen.2013.03.021>.
- [7] L.E. Klebanoff, J.O. Keller, *Int. J. Hydrogen Energy* 38 (2013) 4533–4576.
- [8] C. Paduani, P. Jena, *Int. J. Hydrogen Energy* 38 (2013) 2357–2362.
- [9] Y.P. Pang, Y.F. Liu, X. Zhang, M.X. Gao, H.G. Pan, *Int. J. Hydrogen Energy* 38 (2013) 1460–1468.
- [10] J.F. Mao, Z.P. Guo, X.B. Yu, H.K. Liu, *Int. J. Hydrogen Energy* 38 (2013) 3650–3660.
- [11] F. Yuan, X.W. Chen, Q.F. Gu, Z.W. Tang, X.B. Yu, *Int. J. Hydrogen Energy* 38 (2013) 5322–5329.
- [12] O.V. Komova, V.I. Simagina, N.L. Kayl, G.V. Odegova, O.V. Netskina, Y.A. Chesalov, A.M. Ozerova, *Int. J. Hydrogen Energy* 38 (2013) 6442–6449.
- [13] Z.G. Zhang, H. Wang, J.W. Liu, M. Zhu, *Thermochim. Acta* 560 (2013) 82–88.
- [14] U. Ulmer, J.J. Hu, M. Franzreb, M. Fichtner, *Int. J. Hydrogen Energy* 38 (2013) 1439–1449.
- [15] D.M. Liu, C. Gao, Z.X. Qian, T.Z. Si, Q.A. Zhang, *Int. J. Hydrogen Energy* 38 (2013) 3291–3296.
- [16] X.P. Zheng, J.J. Zheng, Q.H. Ma, S.L. Liu, X. Feng, X.B. Lin, G. Xiao, *J. Alloys Compd.* 551 (2013) 508–511.
- [17] L. Li, F.Y. Qiu, Y.J. Wang, Y.A. Xu, C.H. An, G. Liu, L.F. Jiao, H.T. Yuan, *Int. J. Hydrogen Energy* 38 (2013) 3695–3701.
- [18] Bogdanović, Schwickardi, *J. Alloys Compd.* 253–254 (1997) 1–9.
- [19] X.P. Zheng, G. Xiao, S.L. Liu, X. Feng, J.J. Zheng, *Int. J. Hydrogen Energy* 37 (2012) 8402–8407.
- [20] R.J. Xiong, G. Sang, X.Y. Yan, G.H. Zhang, X.Q. Ye, C.L. Jiang, L.Z. Luo, *Int. J. Hydrogen Energy* 37 (2012) 10222–10228.
- [21] T. Sun, B. Zhou, H. Wang, M. Zhu, *Int. J. Hydrogen Energy* 33 (2008) 2260–2267.
- [22] M. Fichtner, J. Engel, O. Fuhr, O. Kircher, O. Rubner, *Mater. Sci. Eng. B* 108 (2004) 42–47.
- [23] S.Y. Zheng, F. Fang, G.Y. Zhou, G.R. Chen, L.Z. Ouyang, M. Zhu, D.L. Sun, *Chem. Mater.* 20 (2008) 3954–3958.
- [24] J.B. Gao, P. Adelhelm, M.H.W. Verkuijen, C. Rongeat, M. Herrich, P.J.M. van Bentum, O. Gutfleisch, A.P.M. Kentgens, K.P. de Jong, P.E. de Jongh, *J. Phys. Chem. C* 114 (2010) 4675–4682.
- [25] T. Schmidt, L. Röntzsch, *J. Alloys Compd.* 496 (2010) L38–L40.
- [26] Y.P. Wang, Q.L. Ren, Y.J. Wang, L. Li, D.W. Song, L.F. Jiao, H.T. Yuan, *Int. J. Hydrogen Energy* 35 (2010) 11004–11008.
- [27] T. Wang, J. Wang, A.D. Ebner, J.A. Ritter, *J. Alloys Compd.* 450 (2008) 293–300.
- [28] X.P. Zheng, S.L. Liu, D.L. Li, *Int. J. Hydrogen Energy* 34 (2009) 2701–2704.
- [29] T. Wang, J. Wang, A.D. Ebner, J.A. Ritter, *J. Alloys Compd.* 539 (2012) 242–248.
- [30] F.E. Pinkerton, *J. Alloys Compd.* 509 (2011) 8958–8964.
- [31] S.S.-Y. Lin, J. Yang, H.H. Kung, *Int. J. Hydrogen Energy* 37 (2012) 2737–2741.
- [32] G. Streukens, F. Schüth, *J. Alloys Compd.* 474 (2009) 57–60.
- [33] X.L. Fan, X.Z. Xiao, L.X. Chen, S.Q. Li, Q.D. Wang, *J. Alloys Compd.* 509S (2011) S750–S753.
- [34] J. Wang, A.D. Ebner, J.A. Ritter, *Int. J. Hydrogen Energy* 37 (2012) 11650–11655.
- [35] Mehraj-din Naik, Sami-ullah Rather, R. Zacharia, C.S. So, S.W. Hwang, A.R. Kim, K.S. Nahm, *J. Alloys Compd.* 471 (2009) L16–L22.
- [36] J.F. Mao, Z.P. Guo, H.K. Liu, *Int. J. Hydrogen Energy* 36 (2011) 14503–14511.
- [37] M.P. Pitt, P.E. Vullum, M.H. Sørby, M.P. Sulic, H. Emerich, M. Paskevicius, C.E. Buckley, J.C. Walmsley, R. Holmestad, B.C. Hauback, *J. Alloys Compd.* 514 (2012) 163–169.
- [38] Y. Suttisawat, V. Jannatisin, P. Rangsunvigit, B. Kitiyanan, N. Muangsins, S. Kulprathipanja, *J. Power Sources* 163 (2007) 997–1002.
- [39] G.J. Lee, J.H. Shim, Y.W. Cho, K.S. Lee, *Int. J. Hydrogen Energy* 33 (2008) 3748–3753.
- [40] D. Pukazhselvan, M. Sterlin Leo Hudson, A.S.K. Sinha, O.N. Srivastava, *Energy* 35 (2010) 5037–5042.
- [41] L. Li, Y. Wang, F.Y. Qiu, Y.J. Wang, Y.A. Xu, C.H. An, L.F. Jiao, H.T. Yuan, *J. Alloys Compd.* 566 (2013) 137–141.
- [42] L. Li, Y.J. Wang, Y.P. Wang, G. Liu, Y. Han, F.Y. Qiu, C. Yan, D.W. Song, L.F. Jiao, H.T. Yuan, *J. Alloys Compd.* 509S (2011) S747–S749.
- [43] X.L. Fan, X.Z. Xiao, L.X. Chen, L.Y. Han, S.Q. Li, H.W. Ge, Q.D. Wang, *Int. J. Hydrogen Energy* 36 (2011) 10861–10869.
- [44] M.P. Pitt, P.E. Vullum, M.H. Sørby, H. Emerich, M. Paskevicius, C.E. Buckley, E. MacA. Gray, J.C. Walmsley, R. Holmestad, B.C. Hauback, *J. Alloys Compd.* 521 (2012) 112–120.
- [45] F.Q. Zhai, P. Li, A.Z. Sun, S. Wu, Q. Wan, W.N. Zhang, Y.L. Li, L.Q. Cui, X.H. Qu, *J. Phys. Chem. C* 116 (2012) 11939–11945.
- [46] P. Li, Q. Wan, Z.L. Li, F.Q. Zhai, Y.L. Li, L.Q. Cui, X.H. Qu, A.A. Volinsky, *J. Power Sources* 239 (2013) 201–206.
- [47] J.W. Kim, J.H. Shim, S.C. Kim, A. Remhof, A. Borgschulte, O. Friedrichs, R. Gremaud, F. Pendolino, A. Züttel, Y.W. Cho, K.H. Oh, *J. Power Sources* 192 (2009) 582–587.
- [48] Rafi-ud-din, L. Zhang, P. Li, X.H. Qu, *J. Alloys Compd.* 15 (2010) 119–128.
- [49] Rafi-ud-din, X.H. Qu, P. Li, L. Zhang, M. Ahmad, *J. Phys. Chem. C* 115 (2011) 13088–13099.
- [50] S.Y. Zheng, Y.T. Li, F. Fang, C.Y. Zhou, X.B. Yu, G.R. Chen, D.L. Sun, L.Z. Ouyang, M. Zhu, *J. Mater. Res.* 25 (2010) 2047–2053.
- [51] X.Z. Xiao, L.X. Chen, X.H. Wang, S.Q. Li, C.P. Chen, Q.D. Wang, *Int. J. Hydrogen Energy* 33 (2008) 64–73.
- [52] P. Wang, X.D. Kang, H.M. Cheng, *J. Appl. Phys.* 98 (2005) 074905.
- [53] M. Sterlin Leo Hudson, H. Raghubanshi, D. Pukazhselvan, O.N. Srivastava, *Int. J. Hydrogen Energy* 37 (2012) 2750–2755.
- [54] P. Adelhelm, J.B. Gao, M.H.W. Verkuijen, C. Rongeat, M. Herrich, P.J.M. van Bentum, O. Gutfleisch, A.P.M. Kentgens, K.P. de Jong, P.E. de Jongh, *Chem. Mater.* 22 (2010) 2233–2238.
- [55] G.J. Lee, J.H. Shim, Y.W. Cho, K.S. Lee, *Int. J. Hydrogen Energy* 32 (2007) 1911–1915.
- [56] J.C. Bureau, Z. Amri, P. Claudy, J.M. Létoffé, *Mater. Res. Bull.* 24 (1989) 23–31.
- [57] S. Gomes, G. Renaudin, H. Hagemann, K. Yvon, M.P. Sulic, C.M. Jensen, *J. Alloys Compd.* 390 (2005) 305–313.